The vibrational spectra of ice Ih and polar ice

Hiroshi Fukazawa and Shinji Mae

Department of Applied Physics, Faculty of Engineering, Hokkaido University, N13W8, Sapporo 060-8628, JAPAN

Abstract: This article reviews experimental and theoretical work on the dynamics and structure of artificial ice, ice Ih, and natural ice recovered from Antarctic and Greenland ice sheet. We focused on analyses of the vibrational spectra of artificial ice and polar ice. Based on the analyses of the vibrational spectra, which observed by Raman and inelastic neutron scattering measurements, we discussed the motion and arrangement of water molecules in ice.

1. Introduction

Ice Ih is ordinary ice, and the oxygen nuclei in ice Ih have a hexagonal arrangement. The orientations of water molecules are disordered under pressure below about 200 MPa and at temperatures from 0 K to the melting point. Therefore the positions of the protons are disordered following the ice rules: (1) there is only one proton on each bond, and (2) there are only two protons close to each oxygen nucleus. The ice rules were proposed by Pauling based on the calculation of residual entropy [1]. Neutron diffraction measurement of D_2O by Peterson and Levy [2] and of H_2O by Kuhs and Lehmann confirmed the proton-disordered arrangement. Thus, protons in ice Ih are equally distributed among the two possible sites on each O-O bond, as shown in Fig. 1a.

The study of the distribution of protons and the hexagonal arrangement of oxygen nuclei in polar ice is fundamental to the investigation for physical properties of ice core recovered from polar ice sheet. The knowledge of the dynamics and structure of atoms and molecules in polar ice would especially lead to an understanding of the electrical and mechanical properties and the diffusion processes of water molecules and inclusion (chemical constituents, atmospheric gases, and so on) in ice sheet, which is essential for reconstructing the past environment. In the present review, we report dynamics and structure of molecules and atoms in artificial ice, ice Ih, polar ice.

2. The vibrational spectra of ice Ih

The vibrational spectra, which are due to the crystal structure and atomic motions,

Physics of Ice Core Records
Edited by T. Hondoh
Hokkaido University Press, 2000, Sapporo

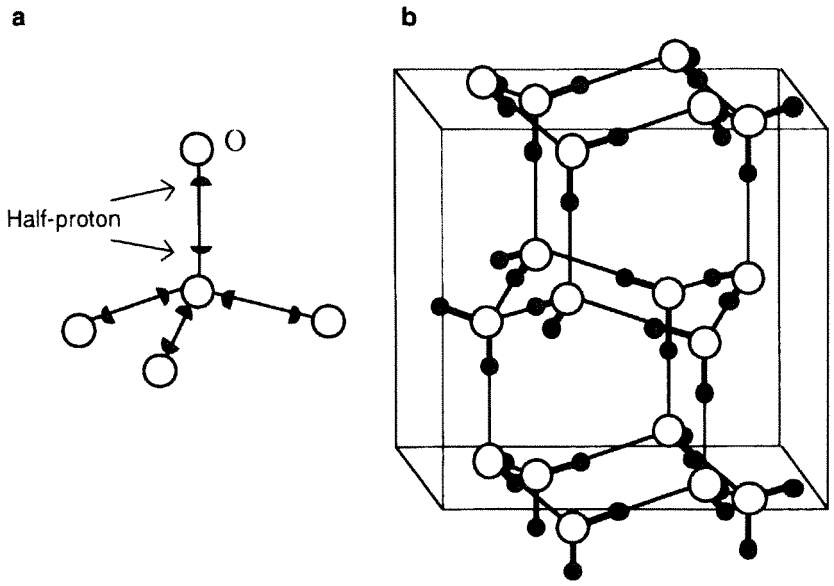

Figure 1: (a) Location of protons in ice Ih as determined by the neutron diffraction pattern [2]. Oxygen nuclei are represented by open circles and protons by shaded half-circles. There are two half-protons along each O-O axis. (b) Structure of ice XI (space group $Cmc2_1$) as determined by the neutron diffraction pattern [20]. Open circles represent oxygen nuclei and shaded circles represent protons.

have been investigated using mainly infrared, Raman and neutron spectroscopy. The infrared absorption is caused by a change of amount of electric dipole moment of molecules. The Raman scattering is made by a strain-dependence of the electronic polarizability. The neutron scattering is made by interaction with the nuclei of the atoms. Since hydrogen has a very large incoherent scattering cross-section (79.7 barns as compared with 0.01 barns of oxygen), the IINS spectrum is sensitive to a change of the arrangement and motion of proton in ice.

Figs. 2a, b and c show the infrared, Raman and incoherent inelastic neutron scattering (IINS) spectra of artificial ice, ice Ih, in the energy range of below 4000 cm^{-1}. The spectra have peaks in the range of 150–350 cm^{-1}, 400–1000 cm^{-1}, and 2800–3200 cm^{-1}, which assigned to translational lattice vibrations, librational vibrations and O-H stretching vibrations, respectively. The translational and librational vibrations are intermolecular mode of vibrations, and O-H stretching vibration is intramolecular mode.

2.1. The translational lattice vibrations

On the basis of the space symmetry in oxygen nuclei, $P6_3/mmc$, the nine zero-wave-vector translational vibrations form $A_{1g} + B_{1g} + B_{2u} + E_{1g} + E_{2g} + E_{2u}$ (Fig. 3) [4]. All these vibrations are forbidden in the infrared (A_{1g}, E_{1g}, E_{2g} vibrations are Raman active). However, the forbidden vibrations are active because the proton-disordered arrangement destroys the hexagonal symmetry, so that, the infrared spectrum has the peak of the translational lattice vibrations in the region of 150–300 cm^{-1}, as shown in Fig. 2a.

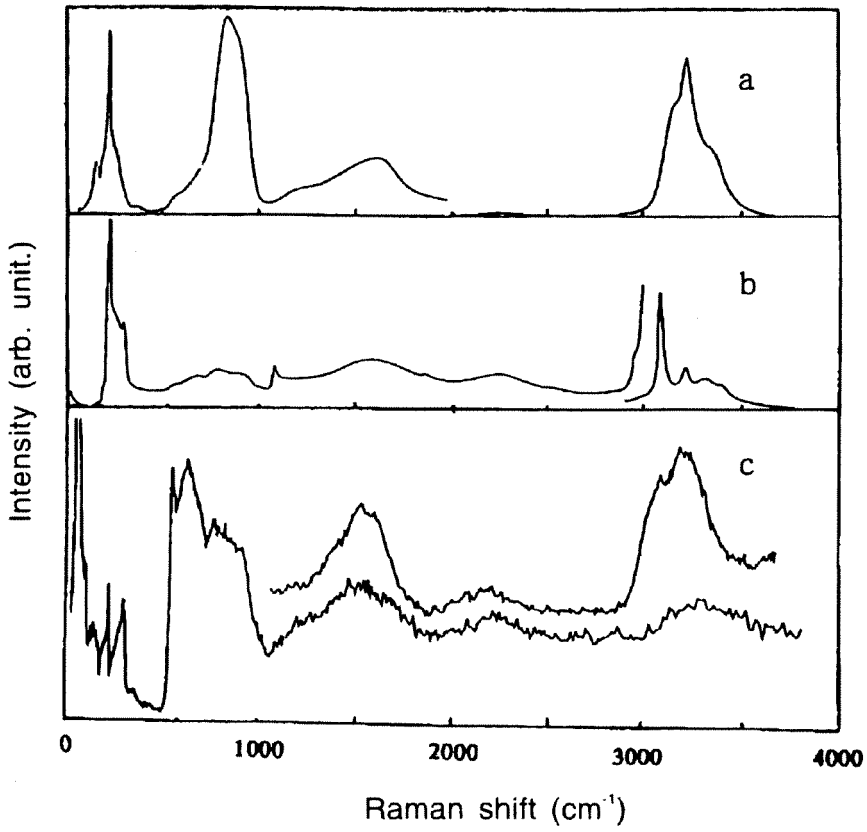

Figure 2: The vibrational spectra of ice Ih measured by infrared (a), Raman (b) and IINS (c) techniques [13]. The upper curve in (c) is the spectrum measured on TFXA and lower curve on HET spectrometer.

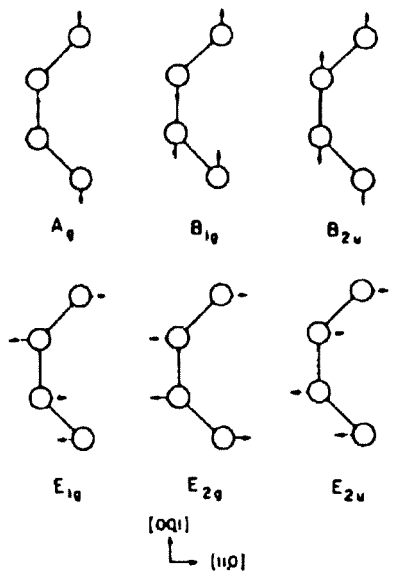

Figure 3: Displacements of the oxygen nuclei in one unit cell in the zone-center vibration of ice Ih [4].

Fig. 4 shows the Raman spectrum of translational lattice vibrations in ice Ih at the measurement temperature of 220–253 K, which has a large peak at about 220 cm^{-1} and a small peak at 300 cm^{-1}. There is a specific density of vibrational states for translational modes at 220 and 300 cm^{-1}. Wong and Whalley [4] discussed the theory of the Raman scattering by the translational lattice vibrations of the proton disordered crystals and showed that the origin of the Raman intensity lies mainly in the disorder in the location of the proton surrounding an hydrogen bond. They concluded that the vibrations above 240 cm^{-1} are connected with the vibrations in the hexagonal symmetry and the peak at 300 cm^{-1} is caused by an electrostatic interaction of the transition moments of neighboring hydrogen bonds. Marchi *et al.* [5] carried out lattice dynamics calculations for ice Ih using the SPC rigid-molecule effective pair

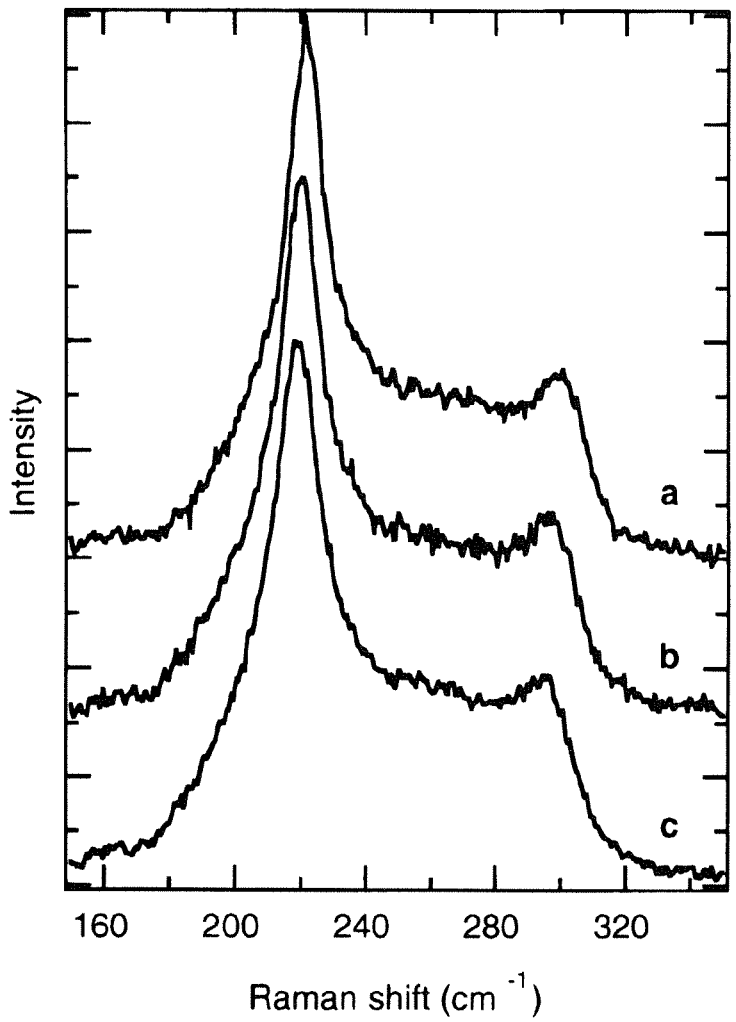

Figure 4: Raman spectra of ice Ih in the region of translational lattice vibrations (150–350 cm^{-1}). Measurement temperatures: (a) 220 K, (b) 238 K and (c) 253 K. The polarization plane of the incident beam was parallel to the c-axis of the sample.

potential with long-range dipole-dipole interactions and calculated the density of states in the translational region. The longitudinal-optic-transverse-optic (LO-TO) analysis of the experimental data combined with the theoretical results of Marchi *et al.* [5] shows that the peak at 220 cm^{-1} is due to TO vibrations and that the peak at 300 cm^{-1} to LO vibrations.

Li and Ross [6] measured the IINS spectra of ice Ih and found two peaks at 27 and 37 meV, respectively, which correspond to the peaks at 220 and 300 cm^{-1} in the Raman spectra. They suggested that the strength of the hydrogen bonds in ice Ih depends on the proton arrangement, and they proposed a model in which weak and strong hydrogen bonds exist randomly in ice Ih in a ratio of about 1 : 2. They carried out lattice dynamics calculations using their model, and they assigned the two peaks at 27 and 37 meV to vibrations traveling across the weak and strong hydrogen bonds, respectively.

In contrast, according to Tse and Klug [7], the peaks at 26 and 35 meV in ice Ih can be reproduced by carefully parameterized intermolecular potentials that include long-range electrostatic interactions without the weak and strong hydrogen bonds. Fukazawa *et al.* [8] also reported that the two peaks at 27 and 37 meV were not due to two different strengths of hydrogen bond on a basis of a comparison of the IINS spectrum of ice Ih and the proton-ordered phase of ice Ih, ice XI.

The sharp peak in the IINS spectrum at about 6 meV is assigned to transverse acoustic vibrations. Ruocco *et al.* [9] measured inelastic the x-ray scattering spectra of ice Ih taken at the indicated valued of momentum transfer, Q. They found that the energy of the acoustic mode increases with increases in Q, and that the energy at Q = 14 nm^{-1} is 27 meV. This result implies that the peak at 27 meV in the vibrational density of state of the ice is related to the acoustic mode.

2.2. The librational vibrations

Bertie and Whalley [10] measured the infrared spectra and absorptivity of ice Ih in the range of 350–4000 cm^{-1}, and the absorption due to the librational vibrations was observed at about 850 cm^{-1}. Wong and E. Whalley [11] reported the Raman spectrum of ice Ih, in which the peak of the librational vibrations at around 800 cm^{-1} was very broad. Klug *et al.* [12] measured the IINS spectrum of ice Ih in the range of 0–160 meV (corresponding to 1290 cm^{-1} in the infrared and Raman spectra) and found a large peak of librational vibrations at 80 meV (640 cm^{-1}). As shown in Fig. 5, librational vibrations are caused by the motion of protons, thus IINS is the measurement technique most sensitive to the vibrations.

The proton ordering greatly affects the shape of the spectra of librational vibrations. The spectra in the proton-disordered phases, ice Ih [8, 12, 13], V [14] and VII [15], are similar, but they differ from those in the proton-ordered phases, ice II [14], VIII [15, 16], IX [14] and XI [8, 17, 18]. Ice Ih and XI are stable below about 200 MPa, while other phases are stable over about 200 MPa. Ice XI is formed in 0.001–0.1-mole KOH-doped ice Ih after being maintained for about 3 days below 72 K [19]. Leadbetter *et al.* [20] measured the powder neutron diffraction of KOD-doped D_2O ice (about 30 % transformation to ice XI) and reported that the arrangement of oxygen nuclei in ice XI is the same as that in ice Ih, but protons in ice XI occupy the ordered position in

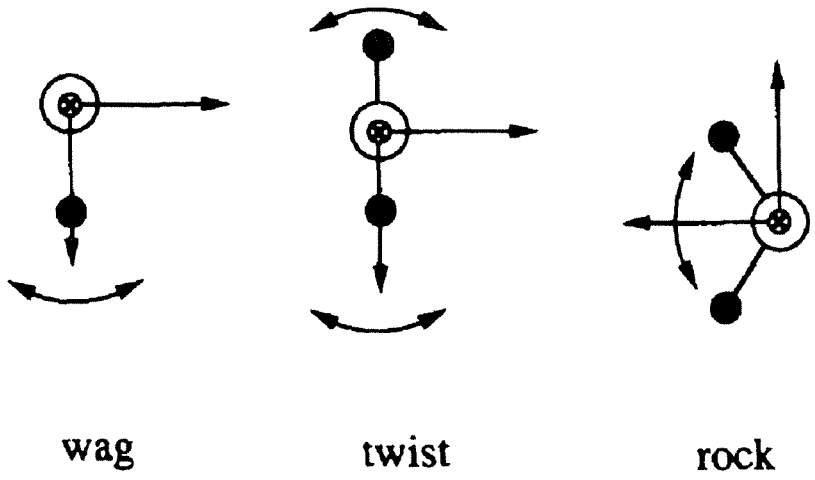

Figure 5: The three librational modes for a water molecules: wag, twist and rock. Oxygen nuclei are represented by open circles and protons by shaded circles [25].

such a way that the spontaneous polarization is parallel to the c-axis (Fig. 1b), thus ice XI is ferroelectric. Howe and Whitworth [21] and Line and Whitworth [22] measured the neutron diffraction of powdered KOH-doped H_2O ice and obtained the polar structure of the space group $Cmc2_1$. Jackson *et al.* [23] also obtained the same result in a neutron diffraction study of a single-crystal of KOH-doped H_2O ice. These results showed that protons in ice Ih are equally distributed among the two possible sites on each O-O bond, while protons in ice XI are fixed at one site on each O-O bond.

Using TFXA and HET spectrometers at the Rutherford Appleton Laboratory, Li *et al.* [17] measured the IINS spectra of 0.02 and 0.055 mole KOH-doped ice sample at 10 K, in which 30–50 % of the protons are ordered. They found that the IINS spectra of the librational vibrations (60–120 meV) of ice XI are clearly different from those of ice Ih: the spectra of ice XI have a strong peak at about 79 meV, but those of ice Ih have a much lower peak, while the difference in the translational lattice vibrations (10–40 meV) between ice XI and ice Ih is small. Itoh *et al.* [24, 25] carried out molecular dynamics simulations and showed that the librational spectra of ice XI have four sharp peaks, but those of ice Ih have broad peaks.

Fukazawa *et al.* [8] measured the IINS spectra of ice Ih and 0.01-mole KOH-doped ice at 21 K (Fig. 6) using a crystal-analyzer time-of-flight (CAT) spectrometer on a pulsed spallation neutron source at the High Energy Accelerator Research Organization (KEK), Japan. In the CAT spectrometer, the scattering angle (θ) is about 0° for an energy of ≥ 20 meV. Based on the analyses of neutron scattering and fermi resonance in hydrogen bonds, Ikeda *et al.* [26] reported the librational vibrations in ice have two components, so that the intensity of the librational mode (40–150 meV) of ice Ih,

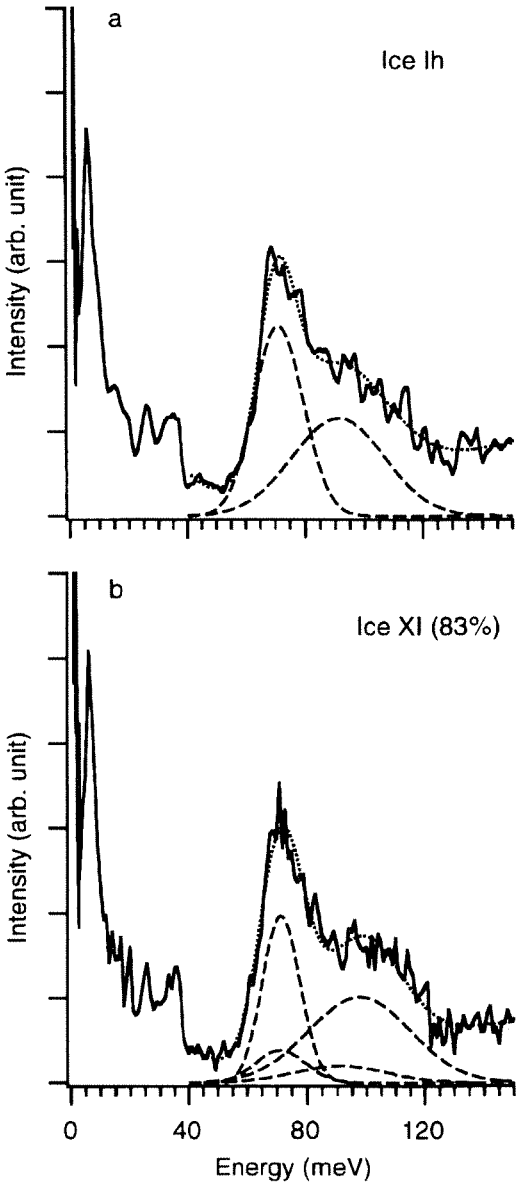

Figure 6: The solid curves represent incoherent inelastic neutron scattering spectra from ice Ih (a) and ice XI (b) in the region of lattice vibrations. The dotted curves are the resultant profiles of the Gaussian functions used for the fittings, indicated by broken curves. Measurements were made at 21 K. The intensities of spectra were normalized by the integrated intensities of the elastic scattering [8].

$I_{Ih}(\varepsilon)$, is written as the sum of two Gaussian functions:

$$I_{Ih}(\varepsilon)=\frac{A_1}{\Gamma_1}\sqrt{4\ln(2)/\pi}\exp\left(\frac{-4\ln(2)(\varepsilon-\varepsilon_1)^2}{\Gamma_1^2}\right)+\frac{A_2}{\Gamma_2}\sqrt{4\ln(2)/\pi}\exp\left(\frac{-4\ln(2)(\varepsilon-\varepsilon_2)^2}{\Gamma_2^2}\right), \quad (1)$$

where A_1 and A_2 are areas, Γ_1 and Γ_2 are FWHM, and ε_1 and ε_2 are energies of the peak centers. Values of parameters are determined by least square fitting (Table 1). The sample of ice XI was a mixture of ice Ih (17 %) and XI (83 %). The intensity of the IINS spectrum of our sample, $I_{XI}(\varepsilon)$, is written as

$$I_{XI}(\varepsilon)=(1-\eta)I_{Ih}(\varepsilon)+\eta\, I_{XI}(\varepsilon)', \quad (2)$$

where $I_{XI}(\varepsilon)'$ is a spectrum of pure ice XI and can be written as the sum of two Gaussian fittings. The value of η is the ratio of ordered protons sample. From electric permittivity, it is estimated that η = 0.83. The fitting shows that Γ_1 and Γ_2 drastically decrease with decreases in η and that the widths of the librational mode strongly depends on the proton ordering.

Ice Ih consists of four configurations of pairs of molecular dipole moments (N_{conf} = 4), while ice XI consists of only two configurations (N_{conf} = 2). Fig. 7 shows the N_{conf} dependence of Γ_1 and Γ_2 of ice, XI and VIII. Ice VIII consists of Bond (D) (N_{conf} = 1). This figure shows that Γ_1 and Γ_2 are proportional to N_{conf}.

Table 1: FWHM (Γ_1 and Γ_2) of two peaks (ε_1 and ε_2) in the libration mode for ice Ih, $I_{Ih}(\varepsilon)$, and ice XI, $I_{XI}(\varepsilon)'$ [8].

	ε_1 (meV)	Γ_1 (meV)	ε_2 (meV)	Γ_2 (meV)	Temperature
$I_{Ih}(\varepsilon)$	71	24	91	44	21K
$I_{XI}(\varepsilon)'$	73	15	97	41	21K
(η = 83 %)					After annealing

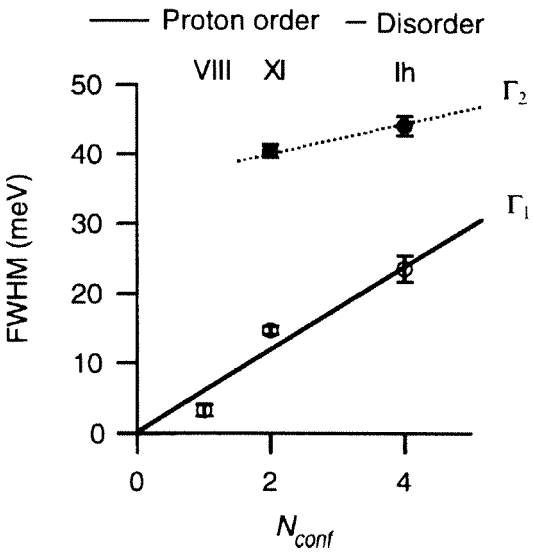

Figure 7: Proton-configuration (N_{conf}) dependence of FWHM (Γ_1 and Γ_2) of ice Ih, XI and VIII [8]. Open and solid circles represent Γ_1 and Γ_2, respectively.

2.3. The O-H stretching vibrations

Bertie *et al.* [27] measured the infrared spectra and absorptivity of ice Ih, and the absorption due to the O-H stretching vibrations was observed at about 3220 cm^{-1}. Wong and Whalley [28] reported the Raman spectrum of ice Ih in the O-H stretching vibration mode (2800–3500 cm^{-1}) and found a strong peak at 3130 cm^{-1} and two weak peaks at 3246 and 3354 cm^{-1}. The peak at 3130 cm^{-1} was assigned to the symmetric stretching vibration mode in-phase vibration, in which the molecules move in phase with one another, and the peaks at 3246 and 3354 cm^{-1} were assigned to the TO-LO splitting of the antisymmetric stretching vibration mode. The Raman spectrum had a broad peak at 1653 cm^{-1}, which was assigned to the H-O-H bending mode, and a peak at 2235 cm^{-1}, which was assigned to the association band of $3\upsilon_L$ (librational mode) or υ_2 (bending mode) + υ_L (librational mode).

Li and Ross [13] measured the spectra in the range of below 500 meV (4000 cm^{-1}). The peak of the O-H stretching vibration at 400 meV (3200 cm^{-1}) was small in the IINS spectrum, because the intensity of IINS decreases with increases in energy.

3. The vibrational spectra of polar ice

3.1. Raman spectra

Dome Fuji (DF) ice was retrieved by the Japanese Antarctic Research Expedition (JARE) at Dome-Fuji station (77°22'S,

39°37'E; elevation 3807 m) at one of the summits in Antarctica in 1995 and 1996 (Fig. 8). Since 1992, a deep ice core drilling project has been carried out by the JARE at this site [29]. In 1997, the drilling reached over 2500 m in depth from the ice sheet surface. The surface temperature is 213 K, and T_i gradually increases with increases in the depth, becoming T_c at a depth of 2060 m. The thickness of the ice at the station was calculated to be about 3060 m by radio echo sounding.

Fukazawa *et al.* [30, 31, 32] investigated the Raman and IINS spectra of ice cores retrieved from Antarctic (Dome Fuji, Vostok, Mizuho and Nansen) and Greenland (Dye-3) ice sheets, because ice in the polar ice sheets had been preserved at a constant temperature for a long period (10^2–10^4 years), and they hypothesized that it is possible to observe a very slow change in the proton arrangement in ice. An incident laser beam with a diameter of 1μm was focused on an appropriate crystal grain

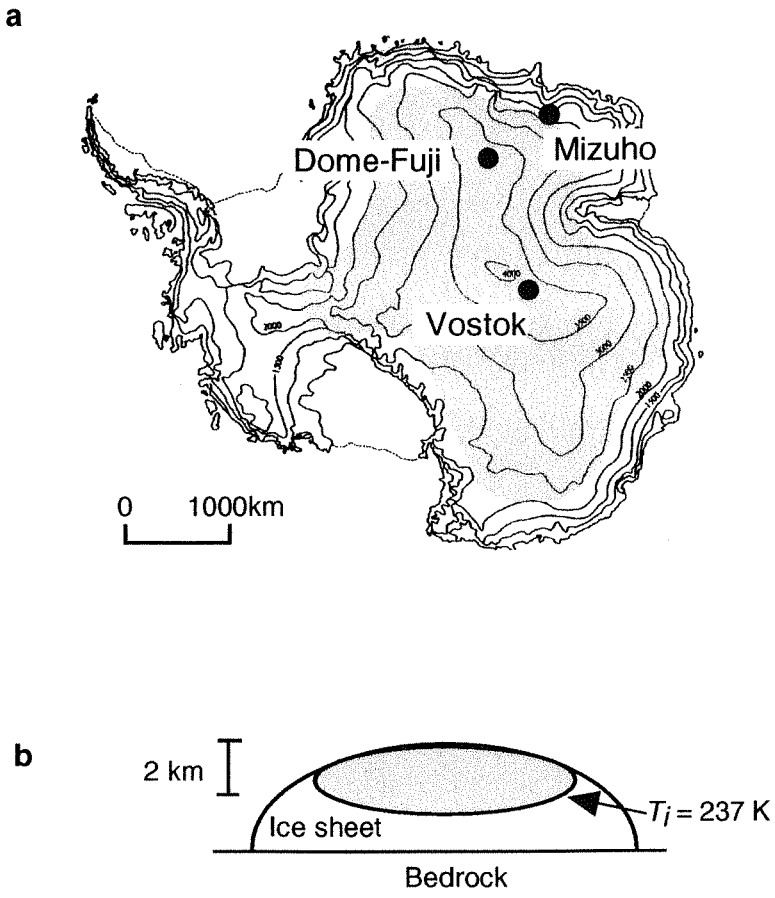

Figure 8: (a) The drilling sites of Dome-Fuji, Mizuho and Vostok ice in Antarctica. The shaded area represents the area where $T_i \leq T_c$ = 237 K on the Antarctic ice sheet surface. (b) Schematic diagram of a cross section of the Antarctic ice sheet. The hatched area shows the area where the ice contains proton-ordered arrangements.

(grain size: 0.5–7.0 mm). The crystal grain was pure ice, because impurities in ice are concentrated at the grain boundaries [33, 34]. They found that the ratio of peak intensities at 300 and 220 cm^{-1} (I_R) was independent of depth (pressure), age of the ice and temperatures at which the measurements were made. However, I_R was dependent on the ice temperature in the ice sheets (T_i). The dependence (Fig. 9a) was as follows: for $T_i \geq T_c = 237$ K, I_R is constant at 0.32 ± 0.01, which is the same as that of the artificial ice (ice Ih); however for $T_i \leq T_c$, I_R decreases with decreases in T_i.

The I_R-T_i relation for $T_i \leq T_c$ and the change in the T_i dependence of I_R at T_c cannot be accounted for by the hypotheses that Klug *et al.* [12] and Li and Ross [6] proposed on the basis of the proton-disordered arrangement of ice Ih. A T_i dependence, such as the I_R-T_i relation, is not found in the Raman spectra of intramolecular vibrations (2800–3600 cm^{-1}) of Antarctic ice. Moreover, x-ray diffraction measurements [35] showed that the structure of oxygen nuclei in Antarctic ice for $T_i \leq T_c$ is the same as that for $T_i \geq T_c$. Therefore, the I_R-T_i relation shown in Fig. 9a is considered to be caused by the proton-ordered arrangement in Antarctic ice samples at values of T_i lower than T_c. Accordingly, I_R is given by

$$I_R = \frac{\sigma_{order}(300)\eta + \sigma_{disorder}(300)(1-\eta)}{\sigma_{order}(220)\eta + \sigma_{disorder}(220)(1-\eta)} \qquad (3)$$

where $\sigma_{order}(220)$ and $\sigma_{order}(300)$ are peak intensities at 220 and 300 cm^{-1}, respectively, due to proton-ordered hydrogen-bonds; $\sigma_{disorder}(220)$ and $\sigma_{disorder}(300)$ are those due to proton-disordered hydrogen-bonds; and η is the ratio of the number of the proton-ordered hydrogen-bonds to that of all hydrogen-bonds. For $T_i \geq T_c$, $I_R = 0.32$ and $\eta = 0$, and, therefore, $\sigma_{disorder}(300) / \sigma_{disorder}(220)$ is 0.32. I_R decreases with decreases in T_i, and we assume that for $T_i \cong 0$ K, $\sigma_{order}(300) = 0$ and $\eta = 1$, based on experimental result about the decrease in I_R. Thus,

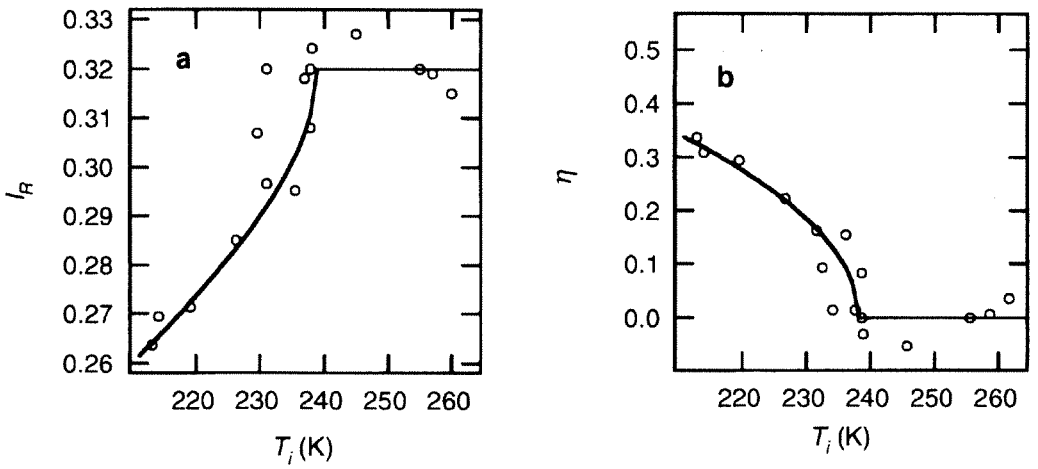

Figure 9: (a) T_i dependence of I_R in Antarctic and Greenland ice [32]. (b) Relation between η and T_i. The solid line shows $\eta = \sqrt{(T_c - T_i)/T_c}$ for $T_i \leq T_c$ and $\eta = 0$ for $T_i \geq T_c$, where $T_c = 237$ K.

$$I_R = \frac{0.32(1-\eta)}{(1-\eta)+C\eta}, \qquad (4)$$

where $C \equiv \sigma_{order}(220) / \sigma_{disorder}(220)$. According to the Landau theory of the second-order phase transition [36], $\eta = \sqrt{(T_c - T_i)/T_c}$ for $T_i \leq T_c$, and $\eta = 0$ for $T_i \geq T_c$, where $T_c = 237$ K. Theoretical values of η are shown by the solid line in Fig. 9b. Substituting the I_R and $C = 0.43$ into Eq. (4), values for η can be calculated, as shown in Fig. 9b (open circles). The plotted values of η are in good agreement with the theoretical values. This analysis shows that about 33 % of the protons in DF ice (T_i = 213 K) are ordered.

3.2. IINS spectra

Proton ordering especially affects the shape of the IINS spectra of librational vibrations. Fukazawa *et al.* [32, 37] measured the IINS spectra of DF and Vostok ice using INC and CAT spectrometers at the KEK. The detectors in the INC are mounted in four banks, and spectra were obtained from the detectors at θ = 30.3–39.8°, and the values of θ are larger than those of CAT spectrometer. DF ice were measured at 21 K, and the IINS spectra obtained (T_i = 213 K and $\eta = 0.33$) are shown in Fig. 10. They then carried out the same measurements for the IINS spectra of ice Ih and 0.01-mole KOH-doped ice, for which a η value of

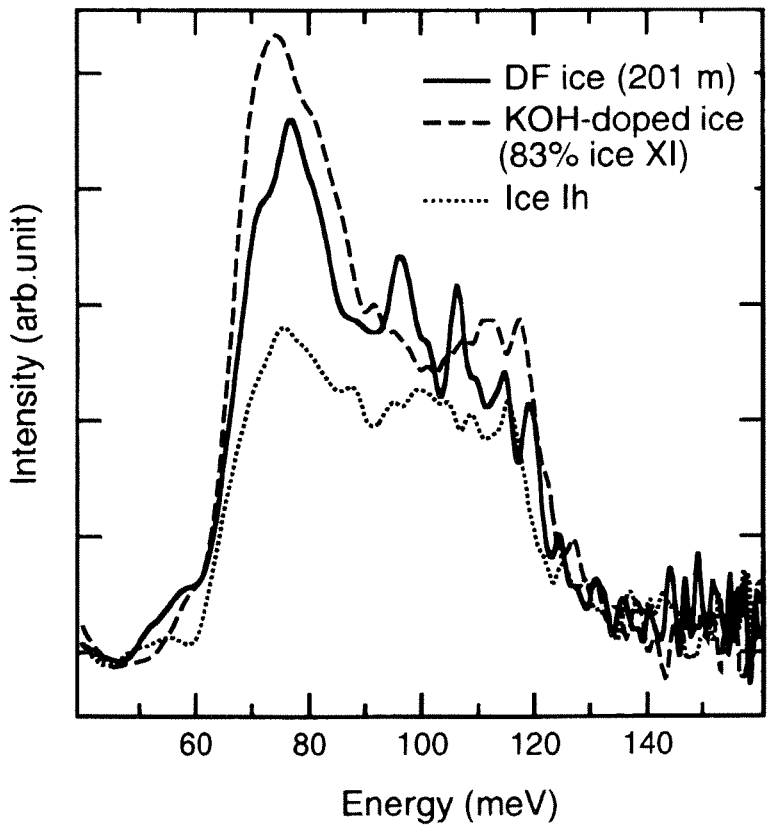

Figure 10: IINS spectra of librational vibrations (Dome-Fuji ice, ice XI, ice Ih) observed by INC spectrometer.

0.83 was estimated, based on electric permittivity measurements [38, 39]. Fig. 10 shows the IINS spectra of ice XI and ice Ih. It was found that both DF ice and ice XI have a sharp peak at about 79 meV, but that the peak of ice Ih is much lower. This result implies that proton-ordered and disordered arrangements coexist in DF ice.

3.3. Ice temperature effect on vibrational spectra of polar ice

The value of η is independent of pressure (i.e., depth) but is dependent on temperature. Since the value of η in DF ice is not influenced by the measurement temperature and the storage temperature of the ice samples after drilling, the value of η is considered to depend on T_i. From the estimation of T_i at each depth using a model of bed specific heat flow [40], η is plotted against T_i. The plotted values of η are in good agreement with the relation between temperature and η in the Landau theory of the second-order phase-transition [36]: $\eta = \sqrt{(T_c - T_i)/T_c}$ for $T_i \leq T_c$, and $\eta = 0$ for $T_i \geq T_c$, where T_c = 237 K. This agreement suggests that the order-disorder phase-transition takes place at T_c = 237 K in the Antarctic ice sheet. Thus, it is reasonable to consider that Antarctic ice in the area where $T_i \leq 237$ K contains proton-ordered arrangements. About one third of the Antarctic ice mass is considered to contain proton-ordered arrangements. As shown in Fig. 8b, the boundary between the proton-ordered and -disordered arrangements is at a depth of about 2000 m. Goodman *et al.* [41] reported that proton rearrangement controlled the glide of ice. Since the proton-rearrangement in proton-ordered ice is extremely slow, it is thought that the flowability of ice discontinuously changes at a depth of about 2000 m.

The order-disorder phase-transition has not been found in experimental studies of artificial ice (pure ice), because it is considered that a thermodynamic equilibrium of protons cannot be attained in a finite period of time due to the extremely slow cooperative process of proton rearrangement [42]. Suga [43] roughly estimated, on the basis of results of extrapolation of the relaxational heat capacity of ice annealed for 624 hours, that proton-ordering in pure ice requires about 10^6 years, and he proposed that ordered ice (pure ice) exists only on the moons of Jupiter and Saturn. However, on the Earth, Antarctic ice has been kept at a constant temperature for a long period of time (10^2–10^5 years). Furthermore, the proton rearrangement in Antarctic ice is in thermodynamic equilibrium. Therefore, the change in the librational vibration in DF ice with depth, which indicates the phase transition in Antarctic ice sheet, is observed.

Based on the results of proton ordering in Antarctic ice, Fukazawa *et al.* [32] estimated that ice slowly grown from vapor at temperatures lower than 237 K has a proton-ordered arrangement because the ice is in thermodynamic equilibrium. Su *et al.* [44] (1998) measured the sum-frequency vibrational spectra of thin layers of ice grown from vapor at about 140 K and found proton ordering in the ice. Iedama *et al.* [45] also found the proton ordering in ice grown from vapor at temperatures of 40–150 K. The results of these recent works imply that ice grown from vapor in the Earth's ozone layer and atmospheric aerosol over Antarctica have a proton-ordered arrangement.

These temperatures at which a proton-ordered arrangement in ice was found, are

higher than the transition temperature of 72 K in KOH-doped ice. Analyses that explain the phase transition and the high transition temperatures are very important to understand the hydrogen bonding of ice, but it is not clear at present. In order to obtain direct evidence of the proton ordering in ice, the determination of proton arrangements in ice by single-crystal neutron diffraction is important.

4. Temperature effects on vibrational spectra of ice

Ermolieff *et al.* [46] measured the Raman spectra of ice Ih over a temperature range 80–250 K in order to detect a possible anomaly in the spectrum near 100 K. Scherer and Snyder [47] measured the Raman scattering intensity of single crystal of ice Ih at several temperatures in order to clarify the anisotropic effects on the force constants associated with the vibrations. Johari *et al.* [48] reported the measurements of the Raman spectra of ice Ih from 25–273 K and found that the change in the permittivity of ice with changes in temperature is consistent with changes in the main frequency of the translational lattice vibrations.

We reported the Raman spectra of ice Ih and Antarctic ice in the temperature range of 198–270 K in order to observe the change in molecular polarizability due to the change in intermolecular potential.

4.1. Ice Ih

Fig. 4 shows typical Raman spectra of ice Ih (single crystal) at measurement temperature of 220, 238 and 253 K in the region of translational lattice vibrations (150–350 cm^{-1}). The Raman spectra at 220 K have a large peak at 221.61 cm^{-1} and a small peak at about 300 cm^{-1}. The large peaks in the spectra at 238 and 253 K are at 220.52 and 218.07 cm^{-1}, respectively.

Fig. 11 shows the temperature, T, dependence of $\upsilon_{T//C}$ and $\upsilon_{T\perp C}$, where $\upsilon_{T//C}$ and $\upsilon_{T\perp C}$ represent the values of the frequency of the large peak at about 220 cm^{-1}, υ_T, for the polarization planes parallel and perpendicular to the c-axis of ice Ih, respectively. Both $\upsilon_{T//C}$ and $\upsilon_{T\perp C}$ decrease with increases in T, and that the rates of decreases in $\upsilon_{T//C}$ and $\upsilon_{T\perp C}$ discontinuously change at the measurement temperature of T_C = 237 K. The following relations (represent by dotted lines in Fig. 11) were obtained:

$$T \geq T_C,\ \upsilon_{T//C}(\mathrm{cm}^{-1}) = -0.13T(\mathrm{K}) + 251.33, \tag{6}$$

$$\upsilon_{T\perp C}(\mathrm{cm}^{-1}) = -0.12T(\mathrm{K}) + 248.41, \tag{7}$$

$$T \leq T_C,\ \upsilon_{T//C}(\mathrm{cm}^{-1}) = -0.07T(\mathrm{K}) + 237.11, \tag{8}$$

$$\upsilon_{T\perp C}(\mathrm{cm}^{-1}) = -0.07T(\mathrm{K}) + 236.56, \tag{9}$$

Fig. 12 shows the T dependence of $\upsilon_{OH//C}$ and $\upsilon_{OH\perp C}$, where $\upsilon_{OH//C}$ and $\upsilon_{OH\perp C}$ represent the frequency of the peak of the O-H stretching vibrations, υ_{OH}, for the polarization planes parallel and perpendicular to the c-axis of ice Ih, respectively. Both $\upsilon_{OH//C}$ and $\upsilon_{OH\perp C}$ linearly increase with increases in T. The following relations (represented by dotted lines in Fig. 12) were obtained:

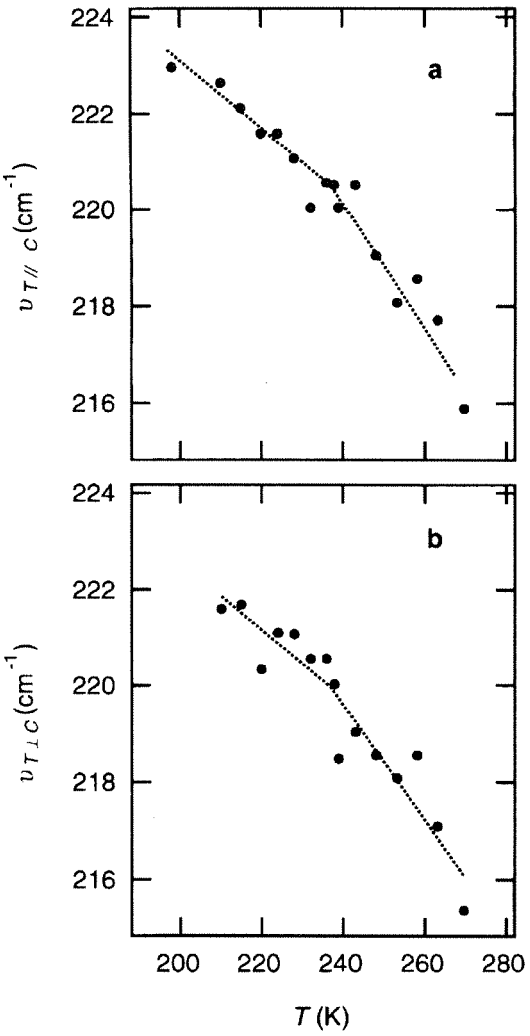

Figure 11: The measurement temperature, T, dependence of the frequency of translational lattice vibrations, υ_T, observed by Raman spectroscopy of the c-axis parallel (a) and perpendicular (b) to the polarization plane of the incident beam.

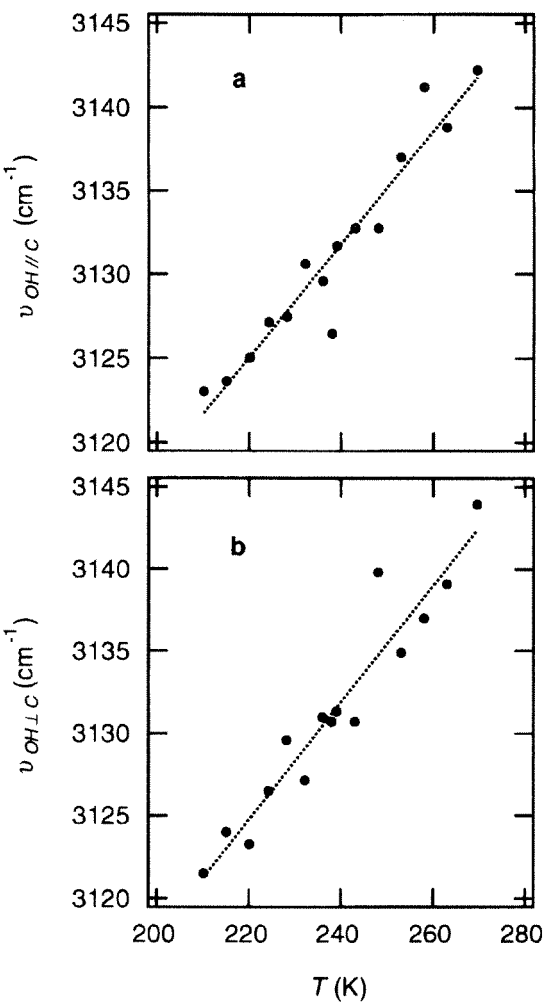

Figure 12: The T dependence of the frequency of the peak of the O-H stretching vibrations, υ_{OH}, observed by Raman spectroscopy of the c-axis parallel (a) and perpendicular (b) to the polarization plane of the incident beam.

$$\upsilon_{OH//C}(\mathrm{cm}^{-1}) = -0.34T(\mathrm{K}) + 3050.76, \quad (10)$$

$$\upsilon_{OH\perp C}(\mathrm{cm}^{-1}) = -0.35T(\mathrm{K}) + 3046.84. \quad (11)$$

The linear increase in υ_{OH} is the same as the T dependence of υ_{OH} reported in a previous work [27].

The lattice constants of the c- and a-axes change with changes in T in the

temperature range of 195–265 K [49]. Thus, the discontinuous changes in $\upsilon_{T//C}$ and $\upsilon_{T\perp C}$ at T_c are caused by a temperature effect at a constant volume, $(\partial\upsilon_T/\partial T)_V$, which is a non-linear effect in the displacement. The value of $(\partial\upsilon_T/\partial T)_V$ is divided into the effect of T on υ_T at constant pressure, $(\partial\upsilon_T/\partial T)_P$, and the constant-temperature volume effect, $(\partial\upsilon_T/\partial P)_T$. Thus,

$$(\partial\upsilon_T/\partial T)_V = (\partial\upsilon_T/\partial T)_P + (\alpha/\beta)(\partial\upsilon_T/\partial P)_T\,, \tag{12}$$

where α is the volume expansivity and β is the compressibility. The values of α and β in ice Ih are 155 MK^{-1} [50] and 12 $Mbar^{-1}$ [51], respectively, at about 255 K. Johari *et al.* [48] reported that $(\partial\upsilon_T/\partial P)_T = 4.77$ cm^{-1} $kbar^{-1}$. Thus, from Eqs. (6), (7), (8) and (9), $(\partial\upsilon_{T//C}/\partial T)_P = -0.13$ $cm^{-1}K^{-1}$ and $(\partial\upsilon_{T\perp C}/\partial T)_P = -0.12$ $cm^{-1}K^{-1}$ for $\geq T_c$, and $(\partial\upsilon_{T//C}/\partial T)_P = -0.07$ $cm^{-1}K^{-1}$ and $(\partial\upsilon_{T\perp C}/\partial T)_P = -0.07$ $cm^{-1}K^{-1}$ for $\leq T_c$, where $(\partial\upsilon_{T//C}/\partial T)_P$ and $(\partial\upsilon_{T\perp C}/\partial T)_P$ are the values of $(\partial\upsilon_T/\partial T)_P$ for the polarization planes parallel and perpendicular to the c-axis of ice Ih, respectively. Substituting these values into Eq. (12):

$$T \geq T_C, \quad (\partial\upsilon_{T//C}/\partial T)_V = -0.07\,, \tag{13}$$

$$(\partial\upsilon_{T\perp C}/\partial T)_V = -0.06\,, \tag{14}$$

$$T \leq T_C, \quad (\partial\upsilon_{T//C}/\partial T)_V = -0.01\,, \tag{15}$$

$$(\partial\upsilon_{T\perp C}/\partial T)_V = -0.01\,, \tag{16}$$

where $(\partial\upsilon_{T//C}/\partial T)_V$ and $(\partial\upsilon_{T\perp C}/\partial T)_V$ are values of $(\partial\upsilon_T/\partial T)_V$ for the polarization planes parallel and perpendicular to the c-axis, respectively. The rates, $(\partial\upsilon_{T//C}/\partial T)_V$ and $(\partial\upsilon_{T\perp C}/\partial T)_V$, below 237 K are about 80 % less than those above 237 K. The decrease at 237 K implies a decrease in the anharmonicity of the lattice vibrations, because $(\partial\upsilon_T/\partial T)_V$ is due to anharmonic term in the intermolecular potential [52]. Sivakumar *et al.* [53] estimated that the anharmonicity is mainly caused by the bending of O-H ··· O angles. The decrease in anharmonicity of the lattice vibrations below 237 K is able to drive phase transitions.

4.2. Polar ice

Figure 13 shows temperature changes in the translational lattice vibrations in DF ice obtained by Raman spectra, υ_T, of the c-axis parallel (a) and perpendicular (b) to the electric field [55]. There are changes at around T_c = 237 K in the rates of decrease of the frequency of the lattice vibrations. The relationship between υ_T and temperature can be written:

$$T \geq T_C,\ \upsilon_T(\mathrm{cm}^{-1}) = -0.136T(\mathrm{K}) + 252.543\,, \tag{17}$$

$$T \leq T_C,\ \upsilon_T(\mathrm{cm}^{-1}) = -0.082T(\mathrm{K}) + 239.985\,, \tag{18}$$

Matsuoka *et al.* precisely measured the temperature dependence of permittivities of pure single-crystal [54] and DF ice (350 m in depth) [55] in the temperature range of 210–260 K. The temperature dependence of real part, ε', in DF ice (Fig. 14) is given by:

$$T \geq T_C, \quad \varepsilon' = 0.0011T + 2.8617\,, \tag{19}$$

$$T \leq T_C, \quad \varepsilon' = 0.0003T + 3.0620\,. \tag{20}$$

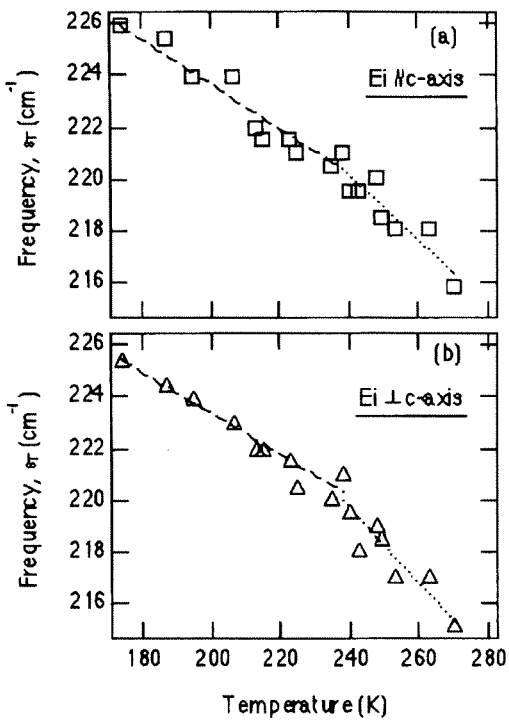

Figure 13: The T dependence of the frequency of translational lattice vibrations in DF ice observed by Raman spectroscopy of the c-axis parallel, (a), and perpendicular, (b), to the electric field [55].

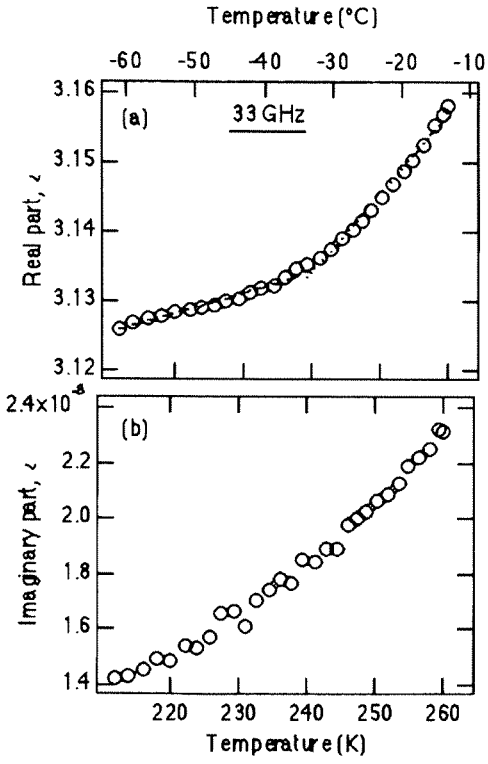

Figure 14: Temperature dependence of permittivities of DF ice core at 33 GHz [55]. (a) real part, ε', (b) imaginary part, ε''.

The measured values of υ_T and ε' are agreement with the Kramers-Krönig relation [48]:

$$\left(\varepsilon'^{1/2} - n_{op}\right)\upsilon_T^2 = \text{const.}, \qquad (21)$$

where n_{op} is the refractive index at optical frequencies. Temperature dependence of n_{op} is governed by the continuous change in the expansivity with changes in temperature. Thus, this agreement implies that the significant change in the rate of decrease of υ_T with temperature at 237 K causes a change in the rate of increase of ε' with temperature and also that of molecular polarizability.

Acknowledgements

We would like to thank Dr. T. Hondoh, Dr. S. Ikeda, Dr. W. F. Kuhs, Dr. V. Ya. Lipenkov and Dr. A. N. Salamatin for their valuable discussions. One of the authors, H. F., has been supported by a Research Fellowship of the Japan Society for the Promotion of Science for Young Scientists.

References

1. L. Pauling, *J. Am. Chem. Soc.*, **57**, 2680 (1935).
2. S.W. Peterson and H.A. Levy, *Acta Crystallogar*, **10**, 70 (1957).

3. W.F. Kuhs and M.S. Lehmann, *Nature*, **294**, 432 (1981).
4. P.T.T. Wong and E. Whalley, *J. Chem. Phys.*, **65**, 82 (1976).
5. M. Marchi, J.S. Tse and M.L. Klein, *J. Chem. Phys.*, **85**, 2414 (1986).
6. J.C. Li and D.K. Ross, *Nature*, **365**, 327 (1993).
7. J.S. Tse and D.D. Klug, *Phys. Lett.*, **198**, 464 (1995).
8. H. Fukazawa, S. Ikeda and S. Mae, *Chem. Phys. Lett.*, **282**, 215 (1998).
9. G. Ruocco, F. Sette, U. Bergmann, M. Krisch, C. Masciovecchio, V. Mazzacurati, G. Signorelli and R. Verbeni, *Nature*, **379**, 521 (1996).
10. J.E. Bertie and E. Whalley, *J. Chem. Phys.*, **40**, 1637 (1964).
11. P.T.T. Wong and E. Whalley, *J. Chem. Phys.*, **62**, 2418 (1974).
12. D.D. Klug, E. Whalley, E.C. Svensson, J.H. Root and V.F. Sears, *Phys. Rev. B*, **44**, 841 (1991).
13. J.C. Li and D.K. Ross, *Proc. Int. Conf. Physics and Chemistry of ice*, 27-34 (1992).
14. J.C. Li, J. D. Londono, D.K. Ross, J.L. Finney, J. Tomkinson and W.F. Sherman, *J. Chem. Phys.*, **94**, 6770 (1991).
15. J.C. Li and M. Adams, *Europhys. Lett.*, **34**, 675 (1996).
16. A.I. Kolesnikov, J.C. Li, D.K. Ross, V.V. Sinitzin, O.I. Barkalov, E.L. Bokhenkov and E.G. Ponyatovskii, *J. Phys. Lett. A*, **168**, 308 (1992).
17. J.C. Li, V.M. Nield and S.M. Jackson, *Chem. Phys. Lett.*, **241**, 290 (1995).
18. J.C. Li, *J. Chem. Phys.*, **105**, 6733 (1996).
19. Y. Tajima, T. Matsuo and H. Suga, *Nature*, **299**, 810 (1982).
20. A.J. Leadbetter, R.C. Ward, J.W. Clark, P.A. Tucker, T. Matsuo and H. Suga, *J. Chem. Phys.*, **82**, 424 (1985).
21. R. Howe and R.W. Whitworth, *J. Chem. Phys.*, **90**, 4450 (1989).
22. C.M.B. Line and R.W. Whitworth, *J. Chem. Phys.*, **104**, 10008 (1996).
23. S.M. Jackson, V.M. Nield, R.W. Whitworth, M. Oguro and C.C. Wilson, *J. Phys. Chem. B*, **101**, 6142 (1997).
24. H. Itoh, K. Kawamura, T. Hondoh and S. Mae, *Physica B*, **219&220**, 469 (1996).
25. H. Itoh, K. Kawamura, T. Hondoh and S. Mae, *J. Chem. Phys.*, **109**, 4894 (1998).
26. S. Ikeda, H. Sugimoto and Y. Yamada, *Phys. Rev. Lett.*, **81**, 5449 (1998).
27. J.E. Bertie, H.J. Labbe and E. Whalley, *J. Chem. Phys.*, **50**, 4501 (1969).
28. P.T.T. Wong and E. Whalley, *J. Chem. Phys.*, **62**, (1975).
29. O. Watanabe, W. Shimada, H. Narita, A. Miyamoto, K. Tayuki, T. Hondoh, T. Kawamura, S. Fujita, H. Shoji, H. Enomoto, T. Kameda, K. Kawada and K. Yokoyama, *Proc. NIPR Symp. Polar Meteorol. Glaciol.*, **11**, 1-8 (1997).
30. H. Fukazawa, T. Ikeda, T. Hondoh, V.Ya. Lipenkov and S. Mae, *Physica B*, **219&220**, 466 (1996).
31. H. Fukazawa, D. Suzuki, T. Ikeda, S. Mae and T. Hondoh, *J. Phys. Chem. B*, **101**, 6184 (1997).
32. H. Fukazawa, S. Mae, S. Ikeda and O. Watanabe, *Chem. Phys. Lett.*, **294**, 554 (1998).
33. R. Mulvaney, E.W. Wolff and K. Oates, *Nature*, **331**, 247 (1988).
34. T. Matsuoka, S. Fujita and S. Mae, *J. Phys. Chem. B*, **101**, 6219 (1997).
35. T. Ikeda, *Master's thesis*, Hokkaido Univ. (1994).

36. L.D. Landau and E.M. Lifshitz, *Statistical Physics*, Pergamon Press, London, 1959.
37. H. Fukazawa, S. Mae, S. Ikeda and V.Ya. Lipenkov, *Polar and Meteology and Glaciology* (in press).
38. M. Oguro and R.W. Whitworth, *J. Phys. Chem. Solids*, **52**, 401 (1991).
39. H. Looyenga, *Physica*, **31**, 401 (1965).
40. A.N. Salamatin, *Data of glaciological studies*, **83**, 227 (1997).
41. D.J. Goodman, H.J. Frost and M.F. Ashby, *Phil. Mag.*, **43**, 665 (1981).
42. D. Eisengerg and W. Kauzmann, *The Structure and Properties of Water*, Oxford Univ. Press, London, 1969, 77pp.
43. H. Suga, *Solid State Physics* (in Japanese), **20**, 125 (1985).
44. X. Su, L. Lianos, Y.R. Shen and G.A. Somorjai, *Phys. Rev. Lett.*, **80**, 153 (1988).
45. M.J. Iedema, M.J. Dresser, D.L. Doering, J.B. Rowland, W.P. Hess, A.A. Tsekouras and J.P. Cowin, *J. Phys. Chem. B*, **102**, 9203 (1988).
46. A. Ermolieff, P. Faure and A. Chasson, *J. Phys. Paris*, **37**, 1457 (1976).
47. J.R. Scherer and R.G. Snyder, *J. Chem. Phys.*, **67**, 4794 (1977).
48. G.P. Johari, H.A.M. Chew and T.C. Sivakumar, *J. Chem. Phys.*, **80**, 5163 (1984).
49. K. Röttger, A. Endriss, J. Ihringer, S. Doyle and W.F. Kuhs, *Acta Cryst. B*, **50**, 644 (1994).
50. S.J. La Place and B. Post, *Acta Crystallographica*, **13**, 503 (1960).
51. A.J. Gow and J. Williamson, *J. Geophys. Res.*, **77**, 6348 (1972).
52. G.P. Johari, *Contemp. Phys.*, **22**, 613 (1981).
53. T.C. Sivakumar, H.A.M. Chew and G.P. Johari, *Nature*, **275**, 524 (1978).
54. T. Matsuoka, S. Fujita, S. Morishima and S. Mae, *J. Appl. Phys.*, **81**, 2344 (1977).
55. T. Matsuoka, S. Mae, H. Fukazawa, S. Fujita and O. Watanabe, *Geophys. Res. Lett.*, **25**, 1573 (1998).

Editor's comment: To better understand the arguments on the new phase transition of ice proposed in this paper, it is recommended to consider also the reviewer's comment: "It seems highly unlikely that protons could order at temperatures as high as 237 K. The Bjerrum defect mobility even in the purest ice would prevent ordering to happen. If, on the other hand, proton ordered ice would be the thermodynamically stable phase below 237 K, the proton mobility is certainly high enough that ordering should occur easily on laboratory time-scales. The anomaly at 237 K thus is very unlikely to originate in proton ordering."